SCIENTIFIC REPORTS
nature research

OPEN

Hepatocyte-specific deletion of *Pparα* promotes NAFLD in the context of obesity

Marion Régnier[1], Arnaud Polizzi[1], Sarra Smati[1,2], Céline Lukowicz[1], Anne Fougerat[1], Yannick Lippi[1], Edwin Fouché[1], Frédéric Lasserre[1], Claire Naylies[1], Colette Bétoulières[1], Valentin Barquissau[2], Etienne Mouisel[2], Justine Bertrand-Michel[3], Aurélie Batut[3], Talal Al Saati[4], Cécile Canlet[1], Marie Tremblay-Franco[1], Sandrine Ellero-Simatos[1], Dominique Langin[2,5], Catherine Postic[6], Walter Wahli[1,7,8], Nicolas Loiseau[1], Hervé Guillou[1*] & Alexandra Montagner[1,2*]

Peroxisome proliferator activated receptor α (PPARα) acts as a fatty acid sensor to orchestrate the transcription of genes coding for rate-limiting enzymes required for lipid oxidation in hepatocytes. Mice only lacking *Pparα* in hepatocytes spontaneously develop steatosis without obesity in aging. Steatosis can develop into non alcoholic steatohepatitis (NASH), which may progress to irreversible damage, such as fibrosis and hepatocarcinoma. While NASH appears as a major public health concern worldwide, it remains an unmet medical need. In the current study, we investigated the role of hepatocyte PPARα in a preclinical model of steatosis. For this, we used High Fat Diet (HFD) feeding as a model of obesity in C57BL/6 J male Wild-Type mice (*WT*), in whole-body *Pparα*- deficient mice (*Pparα*$^{-/-}$) and in mice lacking *Pparα* only in hepatocytes (*Pparα*$^{hep-/-}$). We provide evidence that *Pparα* deletion in hepatocytes promotes NAFLD and liver inflammation in mice fed a HFD. This enhanced NAFLD susceptibility occurs without development of glucose intolerance. Moreover, our data reveal that non-hepatocytic PPARα activity predominantly contributes to the metabolic response to HFD. Taken together, our data support hepatocyte PPARα as being essential to the prevention of NAFLD and that extra-hepatocyte PPARα activity contributes to whole-body lipid homeostasis.

Non alcoholic fatty liver disease (NAFLD) has become a major public health concern worldwide[1]. NAFLD ranges from benign steatosis to non alcoholic steatohepatitis (NASH), which may progress to irreversible damage, such as fibrosis or hepatocarcinoma. The hallmark of NAFLD is an elevated level of neutral lipids, which accumulate as lipid droplets in hepatocytes[2]. Although the aetiology of the disease is not fully understood, it is strongly associated with obesity and type 2 diabetes (T2D). In human NAFLD, the fatty acids that accumulate in hepatocytes originate from dietary fat[3,4], adipose tissue lipolysis and hepatic *de novo* lipogenesis[3]. In T2D, adipose tissue insulin resistance promotes lipolysis, whereas hyperglycaemia combined with hyperinsulinemia sustains hepatic *de novo* lipogenesis[5].

Given the burden of the NAFLD epidemic, identifying molecular players that can be targeted is a rather important issue[6,7]. Moreover, finding drugs that may be used to treat NASH and its progression to irreversible liver disease is a so far unmet medical need to be solved[8,9]. Among drugs currently being tested in clinical trials

[1]Toxalim, INRAE UMR 1331, ENVT, INP-Purpan, University of Toulouse, Paul Sabatier University, F-31027, Toulouse, France. [2]Institut National de la Santé et de la Recherche Médicale (INSERM), UMR1048, Institute of Metabolic and Cardiovascular Diseases, University of Toulouse, Paul Sabatier University, Toulouse, France. [3]Metatoul-Lipidomic Facility, MetaboHUB, Institut National de la Santé et de la Recherche Médicale (INSERM), UMR1048, Institute of Metabolic and Cardiovascular Diseases, Toulouse, France. [4]Service d'Histopathologie Expérimentale Unité INSERM/UPS/ENVT-US006/CREFRE Inserm, CHU Purpan, 31024, Toulouse, cedex 3, France. [5]Toulouse University Hospitals, Laboratory of Clinical Biochemistry, Toulouse, France. [6]Institut National de la Santé et de la Recherche Médicale (INSERM), U1016, Institut Cochin, Paris, France. [7]Lee Kong Chian School of Medicine, Nanyang Technological University Singapore, Clinical Sciences Building, 11 Mandalay Road, Nanyang, Singapore. [8]Center for Integrative Genomics, Université de Lausanne, Le Génopode, Lausanne, Switzerland. *email: herve.guillou@inrae.fr; alexandra.montagner@inserm.fr

are a number of molecules that activate the peroxisome proliferator activated receptors (PPARs)[8,10]. Three PPAR isotypes are known (α, β/δ, and γ), and they are members of the nuclear receptor family, which act as fatty acid sensors that orchestrate transcription in response to a variety of endogenous ligands[10], such as fatty acids[11], fatty acid derivatives[12] and phospholipids[13]. Once activated by the binding of these lipids, PPARs may either induce or repress the expression of their specific target genes. PPARs are influential regulators of genes involved in metabolism in different tissues[14]. Therefore, several pharmacological agonists have been developed, tested in preclinical models of NAFLD[15,16], and are currently being either used or tested in clinical trials for the treatment of metabolic diseases, and especially NAFLD[16].

PPARα is the most abundant PPAR isotype in the healthy liver[17] and in hepatocytes, PPARα regulates the expression of thousands of genes and contributes to the remarkable metabolic flexibility of the liver[18–21]. PPARα is particularly active during suckling[22–24] and fasting[19,20,25–28], two conditions in which fatty acids are a preferred source of energy for the organism. PPARα is also expressed in many other tissues, including skeletal muscle[29], adipose tissues[30–33], intestine[34], heart[35], and kidney[36]. Germline deletion of *Pparα* renders mice susceptible for many metabolic defects including obesity[37], steatosis[37–39], hepatic inflammation[40] and steatohepatitis[41], but not diabetes[42,43]. We have shown recently that a hepatocyte-specific deletion of *Pparα* induces spontaneous steatosis in aging mice and blunts fasting-induced ketogenesis[19,20]. Moreover PPARα is required for the expression of fibroblast growth factor 21 (FGF21)[44,45], a liver-derived hormone with many endocrine[46] and hepatoprotective functions[47,48].

In the present study, we evaluated the importance of hepatocyte PPARα in steatosis associated with diet-induced obesity. We provide evidence that in mice fed a high fat diet (HFD), *Pparα* deletion in hepatocytes is sufficient to promote NAFLD. In addition, analysis of the hepatic transcriptome, lipidome, and metabolome, demonstrated that extrahepatic PPARα activity significantly contributes to metabolic homeostasis in response to HFD consumption.

Results

Hepatic and total *Pparα* deficiencies dissociate HFD-induced obesity and fatty liver from glucose intolerance. Male mice from different genotypes, namely wild-type (*WT*), germline *Pparα*-null ($Ppar\alpha^{-/-}$) and hepatocyte-specific *Pparα*-null ($Ppar\alpha^{hep-/-}$), were fed a low-fat diet (10% fat, CTRL) or a HFD (60% fat) at 8 weeks of age for 10 weeks at thermoneutrality (30 °C). At the beginning of the experiment, the $Ppar\alpha^{-/-}$ mice were already significantly heavier than the *WT* and $Ppar\alpha^{hep-/-}$ mice (Fig. 1a). All mice, independently of the genotype became overweight and gained approximately 15 g in response to HFD consumption (Fig. 1a,b). Moreover, unlike *WT* and $Ppar\alpha^{hep-/-}$ mice, $Ppar\alpha^{-/-}$ mice on CTRL diet also gained significant body weight. Therefore, $Ppar\alpha^{-/-}$ mice became more overweight than $Ppar\alpha^{hep-/-}$ and *WT* mice at thermoneutrality. In CTRL mice, oral glucose tolerance (OGTT) tested after 10 weeks of HFD feeding was similar regardless of the genotype (Fig. 1c,d). In the HFD-fed groups, *WT* mice became glucose intolerant whereas $Ppar\alpha^{hep-/-}$ and $Ppar\alpha^{-/-}$ mice were protected against this intolerance (Fig. 1c,d). These results are consistent with fasted glucose levels that increased in response to HFD only in *WT* mice, but not in $Ppar\alpha^{hep-/-}$ or $Ppar\alpha^{-/-}$ mice (Fig. 1e). Therefore, HFD feeding leads to fasting hyperglycaemia and glucose intolerance in *WT* mice, but not in $Ppar\alpha^{hep-/-}$ and $Ppar\alpha^{-/-}$ mice.

Different biochemical analyses were performed in plasma from fed animals (Fig. 1f). Total cholesterol, LDL-cholesterol, and HDL-cholesterol tended to increase in response to HFD diet in all three genotypes. However, we found that levels of the 3 lipid parameters were higher in the plasma of $Ppar\alpha^{hep-/-}$ mice than plasma from *WT* and $Ppar\alpha^{-/-}$ mice. Triglycerides were elevated in $Ppar\alpha^{-/-}$ mice fed the CTRL diet and the HFD diet. Triglycerides were elevated in response to HFD only in $Ppar\alpha^{hep-/-}$ mice, but were lower in HFD-fed $Ppar\alpha^{-/-}$ mice compared to control diet-fed $Ppar\alpha^{-/-}$ mice. Taken together, our results show that both hepatocyte-specific and whole-body deletions of *Pparα* promote obesity, which is dissociated from glucose intolerance in mice housed at thermoneutrality and fed a HFD.

Hepatic and total *Pparα* deficiencies promote liver steatosis, inflammation, and injury in HFD-induced obesity. First, we performed histological analysis in order to investigate whether the lack of *Pparα* either globally or liver specific was associated with changes in liver integrity (Fig. 2a). We observed that $Ppar\alpha^{hep-/-}$ and $Ppar\alpha^{-/-}$ mice developed steatosis upon CTRL diet feeding. In HFD, steatosis in $Ppar\alpha^{hep-/-}$ and $Ppar\alpha^{-/-}$ mice was much more severe than for WT mice, which is in agreement with their respective liver weight (Fig. 2a,b). To better characterize liver injury, we used the NAFLD activity scoring (NAS)[49] based on the severity of NAFLD and the degree of inflammation (Fig. 2c). This NAS revealed that $Ppar\alpha^{hep-/-}$ and $Ppar\alpha^{-/-}$ mice fed a HFD exhibited increased lipid droplet deposition in the liver (Fig. 2a,c), which is confirmed by measurement of triglyceride liver content (Fig. 2e). NAS and inflammation scoring also revealed that HFD did not significantly increase hepatic inflammation in WT mice contrarily to both $Ppar\alpha^{hep-/-}$ and $Ppar\alpha^{-/-}$ mice for which at least 75% of mice presented a NAS higher or equal to 7 (Fig. 2c,d). In agreement with increased inflammation, HFD significantly increased plasma markers of liver injury (ALT and AST) in $Ppar\alpha^{-/-}$ and $Ppar\alpha^{hep-/-}$ mice (Fig. 2f).

Gene expression profile in *WT*, $Ppar\alpha^{hep-/-}$, and $Ppar\alpha^{-/-}$ mice in response to HFD-induced obesity. Next, we evaluated the hepatic transcriptome expression pattern in response to HFD using microarrays (details of the experiment and results from the microarray are available in Gene Expression Omnibus database by the name GSE123354). Overall, we identified a total of 8860 probes corresponding to 7173 HFD sensitive genes in at least one of the three genotypes (based on adjusted p-value; FDR < 5%, Fig. 3). Hierarchical clustering of genes highlighted 12 clusters showing specific gene expression profiles according to the experimental conditions (Fig. 3a). Four of them (clusters 1, 4, 11 and 12) showed a typical pattern in $Ppar\alpha^{-/-}$ mice compared to $Ppar\alpha^{hep-/-}$ and *WT* mice regardless of diet. Genes from cluster 1 and 4 were up-regulated in $Ppar\alpha^{-/-}$ in

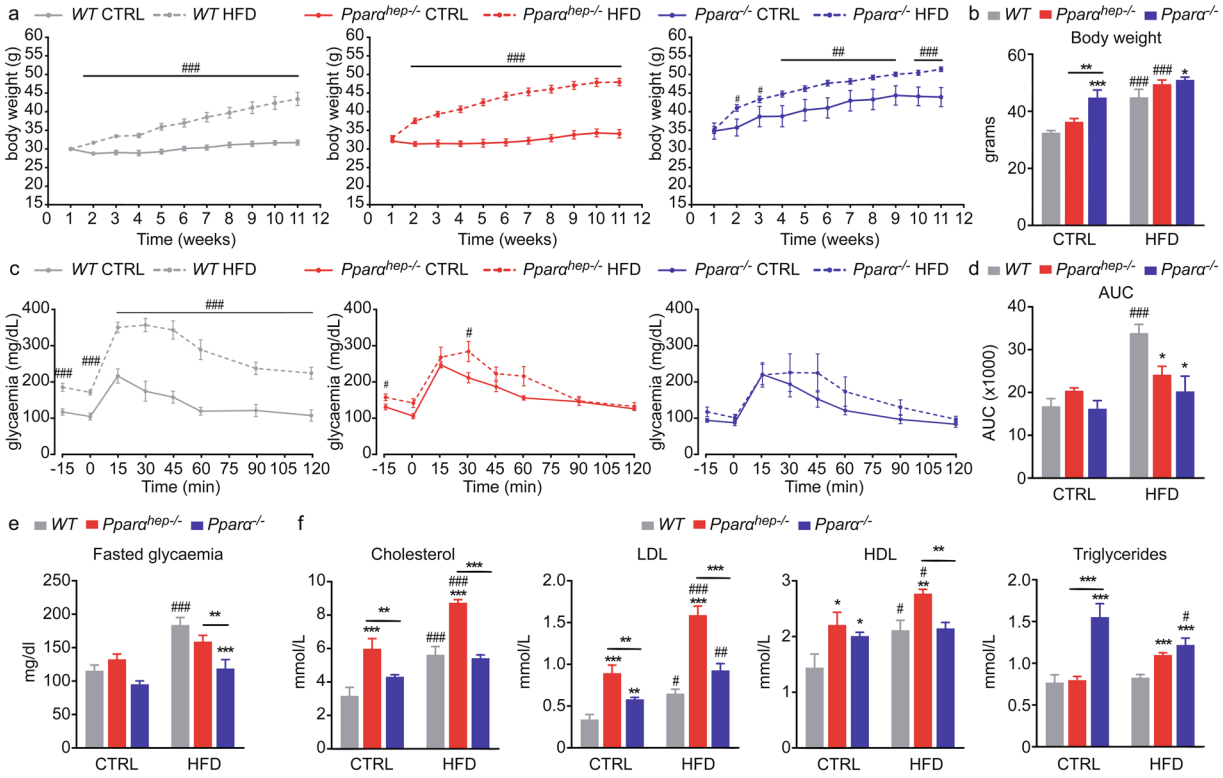

Figure 1. Hepatic and total *Pparα* deficiency does not promote glucose intolerance in HFD- induced obesity. *WT*, *Pparα*$^{hep-/-}$, and *Pparα*$^{-/-}$ mice were fed a control diet (CTRL) or a HFD for 10 weeks at 30 °C (thermoneutrality). (**a**) Body weight gain determined every week during the experiment. (**b**) Body weight at the end of the experiment. (**c**) Blood glucose measured during the oral glucose tolerance test (2 g/kg of body weight). (**d**) Area under the curve obtained after the oral glucose tolerance test. (**e**) Quantification of fasted glycaemia. (f) Plasma cholesterol (total, HDL, and LDL) and triglyceride plasma levels. Data represent mean ± SEM. #, significant diet effect and *, significant genotype effect. $^{\#}$ or *p ≤ 0.05; ## or **p ≤ 0.01; $^{\#\#\#}$ or ***p ≤ 0.001.

comparison to *Pparα*$^{hep-/-}$ and *WT* mice. On the contrary, genes from cluster 11 and 12 were down-regulated in *Pparα*$^{-/-}$. The analysis of gene categories differentially expressed in *Pparα*$^{-/-}$ as compared to *Pparα*$^{hep-/-}$ and *WT* mice highlight the down-regulation of genes associated with PPAR signalling and metabolic homeostasis (Supplementary Figure 1).

Cluster 8 highlighted genes common between *Pparα*$^{-/-}$ and *Pparα*$^{hep-/-}$ mice but distinct from *WT* mice regardless of diet. Interestingly, HFD influences the liver transcriptome in a genotype-specific manner (clusters 2, 5, 6, 9 and 10). The sparse Partial Least Square Discriminant Analysis (sPLS-DA) shows that, although *Pparα*$^{-/-}$ mice liver gene expression profile is clearly different from others, there is also a marked effect of the diet in mice from the 3 genotypes (Fig. 3b). Moreover, the gene expression profile in the liver of HFD-fed mice revealed that: i) the response in *WT* mice is very different from *Pparα*$^{-/-}$ and *Pparα*$^{hep-/-}$ mice; ii) *Pparα*$^{-/-}$ and *Pparα*$^{hep-/-}$ mice have a closer response to HFD (Fig. 3c). Representative qPCR measurements of different gene expression are in line with the microarray analysis (Fig. 3d). The expression of *Vnn1*, encoding a liver-enriched oxidative stress sensor involved in the regulation of multiple metabolic pathways[50], was identified as an HFD-responsive gene specific to the *WT* mice. *Fmo3*, involved in trimethylamine N-oxide (TMAO) production, was identified as an HFD-induced gene specifically in *Pparα*$^{-/-}$ mice. HFD increases the expression of collagen *Col1a1* in the absence of hepatocyte-specific or whole-body *Pparα* but not in *WT* mice. Lastly, *Ppar-γ2* was identified as an HFD-responsive gene common to the three mouse genotypes. We counted 354 hepatic genes responsive to HFD common to the three mouse genotypes (Fig. 3e). These genes are mostly involved in metabolic responses to HFD which do not depend on PPARα (Supplementary Figure 2).

PPARα-dependent changes in hepatic gene expression profiles in response to HFD-induced obesity. We next analysed the genes dependent on *Pparα*. A large group of 1749 Differentially Expressed Genes (DEGs) includes 922 genes significantly up-regulated and 827 significantly down-regulated by HFD feeding only in *WT* mice (Fig. 4a). Examples of these genes include well-established PPARα targets, such as *Cyp4a14*, *Acot3*, *Acot2*, and *Fitm1* (Fig. 4b), and 8 categories of genes involved in metabolism (Fig. 4c) with up-regulated expression in response to a HFD only in *WT* mice. However, we also identified five KEGG categories down-regulated in response to HFD specifically in *WT* mice. These categories relate to RNA transport, ribosome activity and protein processing (Fig. 4d).

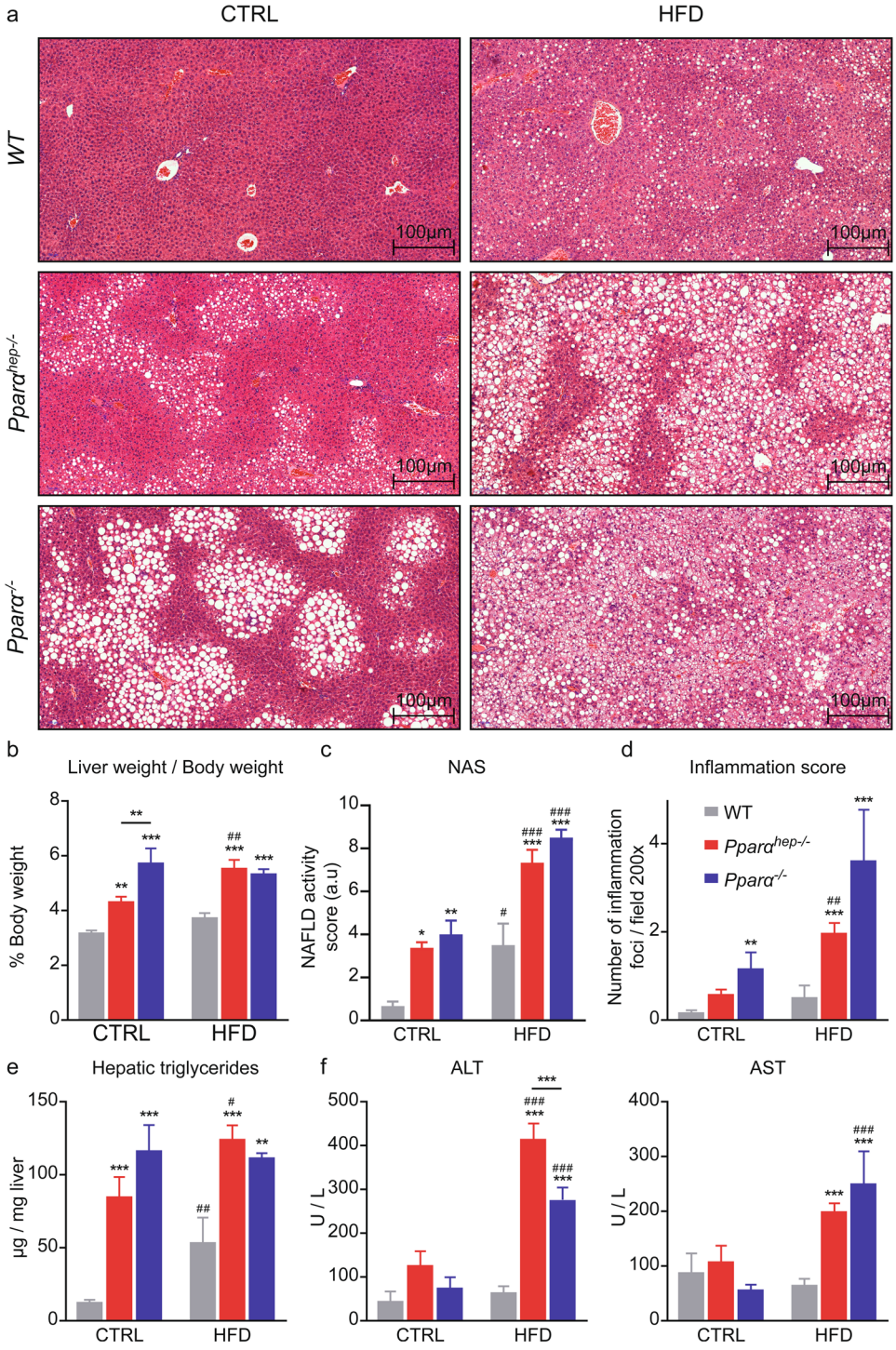

Figure 2. Hepatic and total *Pparα* deficiency promote liver steatosis and inflammation in HFD-induced obesity. *WT*, *Pparα*$^{hep-/-}$, and *Pparα*$^{-/-}$ mice were fed a control diet (CTRL) or a HFD for 10 weeks at 30 °C (thermoneutrality). (**a**) Representative pictures of Haematoxylin and Eosin staining of liver sections. Scale bars, 100 µm. (**b**) Liver weight as a percentage of body weight. (**c**) NAFLD activity score (NAS). (**d**) Histological scoring of inflammation foci in 10 distinct areas at 200×. (**e**) Quantification of hepatic triglycerides (**f**) Plasma ALT and AST. Data represent mean ± SEM. #, significant diet effect and *, significant genotype effect. $^{\#}$ or *$p \leq 0.05$; ## or **$p \leq 0.01$; $^{\#\#\#}$ or ***$p \leq 0.001$.

Then, we questioned whether hepatocyte and wholebody deletion of *Pparα* (*Pparα*$^{-/-}$ and *Pparα*$^{hep-/-}$ mice) induces overlapping responses in HFD-induced obesity. We identified a group of DEGs including 337 and 349 genes significantly up-regulated or down-regulated, respectively, by HFD feeding in both *Pparα*$^{-/-}$ and

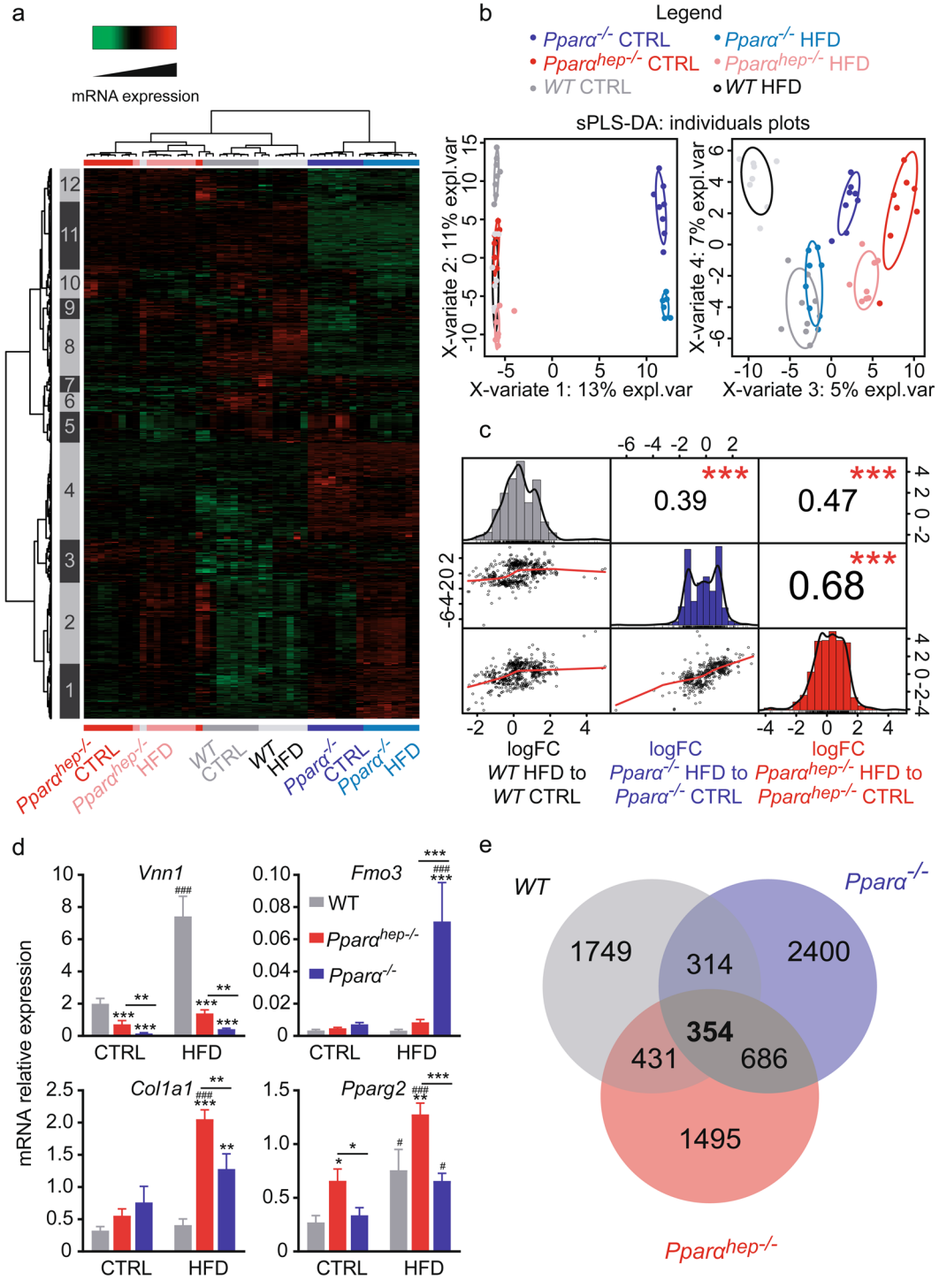

Figure 3. Analysis of the liver transcriptome in *WT*, *Pparα*$^{hep-/-}$, and *Pparα*$^{-/-}$ mice in response to HFD. *WT*, *Pparα*$^{hep-/-}$, and *Pparα*$^{-/-}$ mice were fed a control diet (CTRL) or a HFD for 10 weeks at 30 °C (thermoneutrality). A transcriptomic analysis performed with liver samples from *WT*, *Pparα*$^{hep-/-}$, and *Pparα*$^{-/-}$ exposed or not exposed to HFD (n = 8 mice/group) revealed 7173 differentially regulated genes (FDR < 5%). (**a**) Heat map of microarray expression data from 7173 regulated genes. Red and green indicate values above and below the mean averaged centred and scaled expression values (Z-score), respectively. Black indicates values close to the mean. According to the probe clustering (left panel), 12 gene clusters exhibited specific gene expression profiles. (**b**) sPLS-DA representing the 7173 differentially expressed genes from the microarray. (**c**) Correlation analysis between either *WT*, *Pparα*$^{hep-/-}$, and *Pparα*$^{-/-}$ mice for the effect of HFD. (**d**) Relative hepatic expression of Vnn1, Fmo3, Col1a1 and Pparγ2 quantified by qPCR. Data represent mean ± SEM. #, significant diet effect and *, significant genotype effect. # or *p ≤ 0.05; ## or **p ≤ 0.01; ### or ***p ≤ 0.001. (**e**) Venn diagrams comparing the number of genes significantly regulated under HFD in the livers of *WT*, *Pparα*$^{hep-/-}$, and *Pparα*$^{-/-}$ mice at adjusted p-value < 0.05.

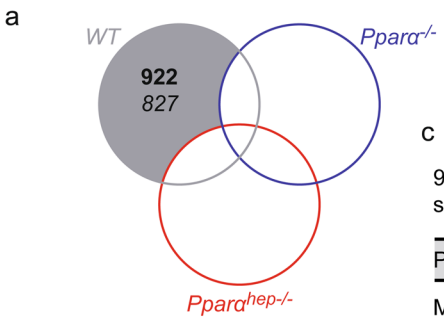

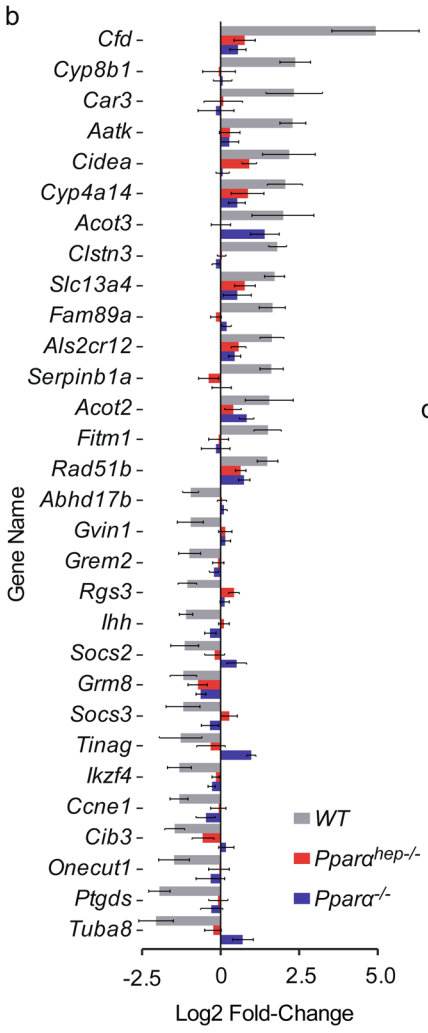

c

9 KEGG categories up-regulated in response to HFD specifically in WT

Pathway description	Genes	p-value
Metabolic pathways	109	1.47e-14
Peroxisome	16	2.36e-05
Thermogenesis	25	7.48e-05
Biosynthesis of unsaturated FA	9	0.00013
Glyoxylate and dicarboxylate metabolism	9	0.00017
FA elongation	8	0.00052
Steroid biosynthesis	7	0.00060
Val, Leu and Ileu degradation	10	0.0017
Retrograde endocannabinoid signaling	15	0.0084

d

5 KEGG categories down-regulated in response to HFD specifically in WT

Pathway description	Genes	p-value
Ribosome	30	2.84e-14
RNA transport	18	0.00056
Ribosome biogenesis in eukaryotes	12	0.00057
Protein processing in endoplasmic reticulum	16	0.0029
mRNA surveillance pathway	11	0.0074

Figure 4. PPARα-independent changes in hepatic gene expression profiles in response to HFD. *WT*, *Pparα*$^{hep-/-}$, and *Pparα*$^{-/-}$ mice were fed a control diet (CTRL) or a HFD for 10 weeks at 30 °C (thermoneutrality). (**a**) Venn diagram presenting the number of hepatic genes over-expressed (bold) and down-regulated (regular) in response to HFD in *WT*, *Pparα*$^{hep-/-}$, *Pparα*$^{-/-}$ mice (FDR < 5%) (**b**) Grey bars represent the top 15 specifically induced and repressed genes between *WT* exposed to CTRL diet and *WT* exposed to HFD. Red and blue bars represent the profile in *Pparα*$^{hep-/-}$ and *Pparα*$^{-/-}$ mice, respectively. (**c**) Gene Ontology (GO) enrichment analysis ($p \leq 0.01$) of KEGG categories based on functional interactions specifically down-regulated in *WT* mice fed a HFD using the String database. (**d**) Gene Ontology (GO) enrichment analysis (adjusted p-value; $p \leq 0.01$) of KEGG categories (based on functionally interactions) up-regulated in *WT* mice fed a HFD the using string database.

Pparα$^{hep-/-}$ mice (Fig. 5a). Gene category analysis did not reveal any functions related to the 349 down-regulated genes by HFD feeding in *Pparα*$^{-/-}$ or *Pparα*$^{hep-/-}$ mice. However, gene category analysis highlighted the functions related to the 337 genes significantly up-regulated by HFD feeding in both *Pparα*$^{-/-}$ and *Pparα*$^{hep-/-}$ mice

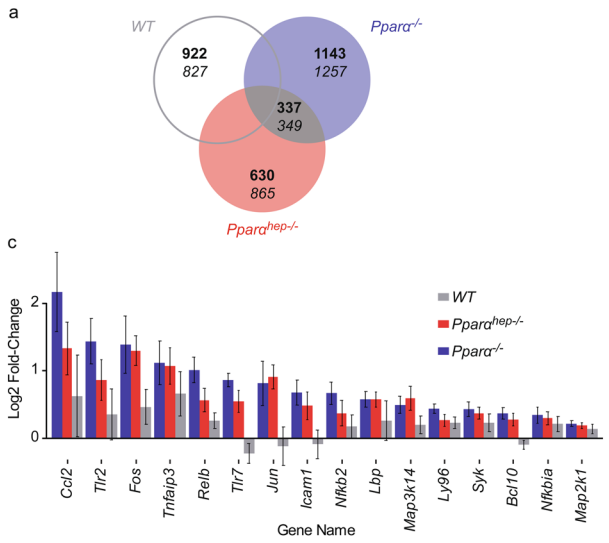

b

12 KEGG categories up-regulated in response to HFD specifically in *Pparα*$^{-/-}$ and in *Pparα*$^{hep-/-}$(p<0.01)

Pathway description	Genes	p-value
Lysosome	16	1.61e-09
Osteoclast differentiation	13	1.08e-06
NF-Kappa B signaling pathway	10	2.67e-05
TNF signaling pathway	10	0.00011
TLR signaling pathway	9	0.000366
Chagas disease	9	0.000366
Phagosome	11	0.000373
Rheumatoid arthritis	8	0.000385
Leishmaniasis	7	0.000625
Epstein-Barr virus infection	10	0.00825
B cell receptor signaling	6	0.00825
Influenza A	9	0.00825

Figure 5. Hepatocyte PPARα prevents liver inflammatory gene expression in response to HFD. *WT*, *Pparα*$^{hep-/-}$, and *Pparα*$^{-/-}$ mice were fed a control diet (CTRL) or a HFD for 10 weeks at 30 °C (thermoneutrality). (**a**) Venn diagram highlighting the number of hepatic genes over-expressed (bold) and down-regulated (regular) in response to HFD specifically in both *Pparα*$^{hep-/-}$ and *Pparα*$^{-/-}$ mice (FDR < 5%). (**b**) Gene Ontology (GO) enrichment analysis (adjusted $p \leq 0.01$) of KEGG categories specifically up-regulated in both *Pparα*$^{hep-/-}$ and *Pparα*$^{-/-}$ mice fed a HFD. (**c**) Gene expression profile of genes identified as being involved in NF-kappa B, TNF and TLR signalling pathways in KEGG.

(Fig. 5b), suggesting that these genes are negatively regulated by PPARα. Most of these categories relate to the inflammatory process, including the NF-kappa B, TNF, and TLR signalling pathways. We selected the genes directly related to these pathways using the KEGG database and the gene database network (Supplementary Figure 3) and confirmed a marked up-regulation of genes belonging to NF-kappa B, TNF, and TLR in the hepatocyte-specific or whole-body absence of *Pparα* (Fig. 5c), in accordance with inflammatory markers measured (Fig. 2c,d).

Specific effect of hepatocytic PPARα and whole body PPARα deletion on liver gene expression in response to HFD-induced obesity. The venn diagram (Fig. 3e) also reveals a large group of DEGs modulated only in *Pparα*$^{hep-/-}$ mice fed a HFD compared to CTRL diet which encompassed 630 and 865 significantly up or down-regulated genes, respectively (Supplementary Figure 4). Figure 3e also defines another large group of DEGs including 1143 and 1257 genes significantly up-regulated and down-regulated, respectively, by HFD feeding only in *Pparα*$^{-/-}$ mice (Supplementary Figure 5). This suggests that the hepato-specific and whole-body deletions of *Pparα* have distinct and specific consequences in the hepatic response to HFD-induced obesity.

To further investigate their specific response, we first indentified the enriched terms across hepatic genes significantly responsive to HFD feeding in *Pparα*$^{hep-/-}$ mice only (Fig. 6a). This analysis highlights metabolic pathways as significantly enriched (Fig. 6a) and a main network (Fig. 6b) including genes related to isoprenoid metabolism and cholesterol synthesis. Second, we analyzed the enriched terms across hepatic genes significantly responsive to HFD feeding in *Pparα*$^{-/-}$ mice but not in WT nor in *Pparα*$^{hep-/-}$ mice (Fig. 6c). This analysis highlight pathways related to metabolism, hemostasis and inflammation as significantly enriched (Fig. 6c) and a main network (Fig. 6d) mostly including genes related to inflammation as well as cell morphology, adhesion and migration.

Metabolic and lipidomic profiling of PPARα-dependent regulation of hepatic homeostasis in response to HFD. We performed unbiased hepatic metabolomic profiling of aqueous metabolites using proton nuclear magnetic resonance (^{1}H-NMR). We used a projection to latent structures for discriminant analysis (PLS-DA) to investigate whether there was a separation between experimental groups of observations. A valid and robust PLS-DA model was obtained that discriminated HFD-fed *Pparα*$^{-/-}$ mice from all other groups (Supplementary Figure 6), further supporting the role of non-hepatocytic PPARα activity in liver homeostatic response to HFD.

We also performed a targeted analysis of 75 lipid species including neutral lipids (cholesterol, cholesterol esters, and triglycerides), phospholipids, and sphingolipids (Fig. 7). The relative abundance of each species in the livers of *WT*, *Pparα*$^{-/-}$, and *Pparα*$^{hep-/-}$ mice fed one of the two diets (CTRL and HFD) was evaluated to determine the contribution of hepatocyte and whole body PPARα activity to hepatic lipid homeostasis. The results are presented as a heatmap with hierarchical clustering (Fig. 7a), in which we observed that the samples first clustered according to the diet, demonstrating that HFD-feeding was the main discriminating factor for hepatic lipid content. We identified four main clusters of lipids with distinct profiles relative to the different experimental conditions. Lipids in cluster 1, such as the ceramides d18:1/C18:1, d18:1/C18:0, and d18:1/C26:0 (Fig. 7b), exhibit

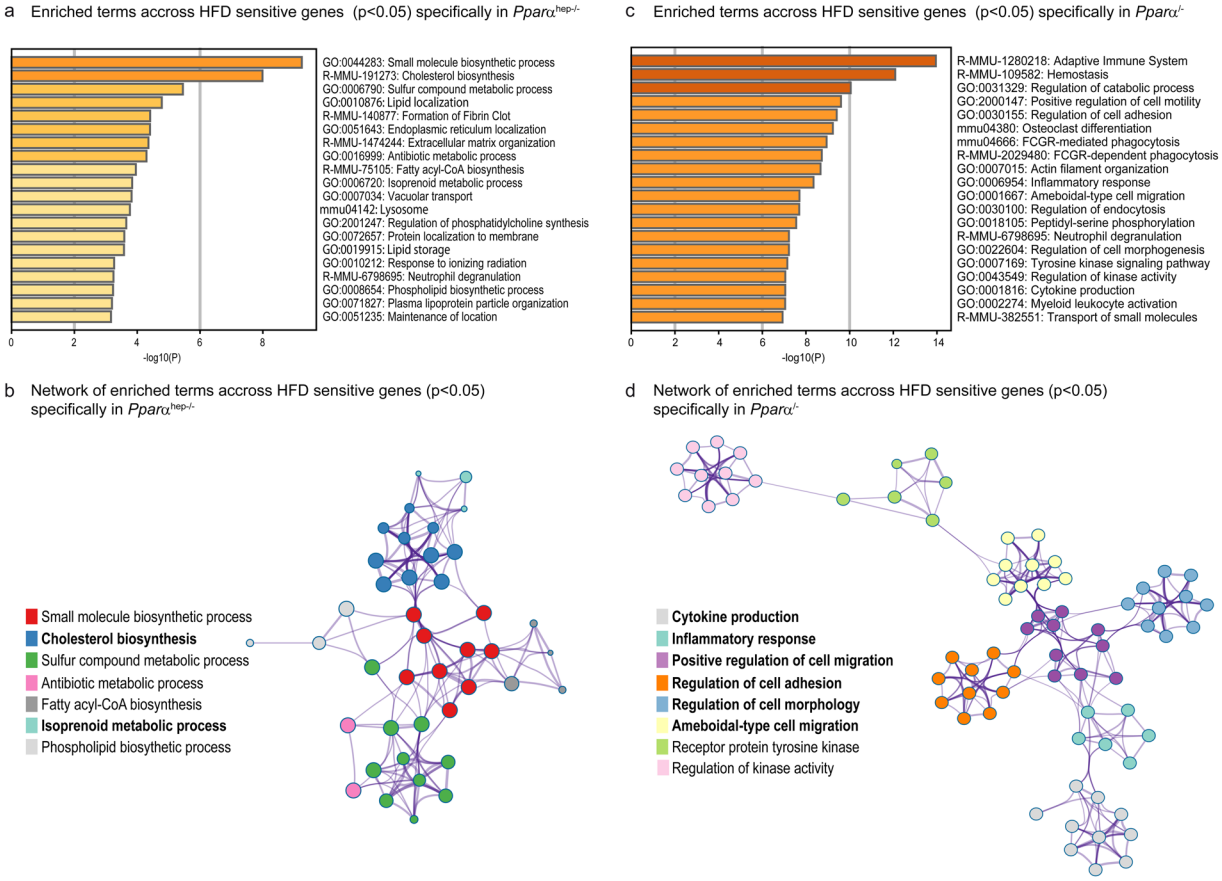

Figure 6. Specific effect of hepatocytic PPARα and whole body PPARα expression on liver gene expression in response to HFD-induced obesity. *WT*, *Pparα*$^{hep-/-}$, and *Pparα*$^{-/-}$ mice were fed a control diet (CTRL) or a HFD for 10 weeks at 30 °C (thermoneutrality). (**a**) Enriched terms across HFD sensitive genes ($p < 0.05$) only in *Ppar*$^{hep\alpha-/-}$ mice (**b**) Network of enriched terms across HFD sensitive genes ($p < 0.05$) only in *Ppar*$^{hep\alpha-/-}$ mice (**c**) Enriched terms across HFD sensitive genes ($p < 0.05$) only in *Pparα*$^{-/-}$ mice d) Network of enriched terms across HFD sensitive genes ($p < 0.05$) only in *Pparα*$^{-/-}$ mice.

increased relative abundance in HFD-fed *Pparα*$^{-/-}$ mice, suggesting that extra-hepatocytic PPARα contributes predominantly to lipid remodelling during HFD-feeding. Cluster 1 also contains linoleic acid (C18:2n-6), which exhibits increased abundance in HFD-fed *Pparα*$^{-/-}$ mice, but also in HFD-fed *Pparα*$^{hep-/-}$ mice. Lipids in cluster 2, such as the phospholipids PC36:3, PC28:6, PE38:4, and triglyceride TG C57 (Fig. 7c), are less abundant in HFD *Pparα*$^{-/-}$ mice. Lipids in cluster 3, such as the palmitoleic acid (C16:1n-7) and PE32:1 (Fig. 7d), are less abundant in HFD mice from the three genotypes. Lipids in cluster 4 (Fig. 7e), such as the polyunsaturated fatty acids C20:4n-6 and C22:5n-3 are more abundant in WT mice from the CTRL diet group and reduced in the livers of mice fed a HFD.

Overall, this lipidomic profiling highlights that the hepatic lipidome depends on both the genotype and diet. Therefore, both hepatic *Pparα* and whole body *Pparα* deletions result in a specific lipidomic response to HFD feeding. However, whole body *Pparα* deficiency has a stronger influence on the effect of HFD-induced obesity on liver metabolic homeostasis.

Discussion

NAFLD is the hepatic manifestation of the obesity epidemic and represents a major public health issue worldwide[51]. NAFLD ranges from benign steatosis to NASH and may promote liver fibrosis and cancer. Therefore, there is a great interest in drugs that could be used to cure NAFLD or reverse NASH before it promotes irreversible damage[8]. PPARα, and other PPAR isotypes represent targets currently being tested in clinical trials[10,52,53]. PPARα is a ligand-activated nuclear receptor that plays a key role in the regulation of metabolic homeostasis by modulating the expression of rate-limiting enzymes involved in fatty acid degradation[18–20]. Preclinical studies in *Pparα*-null mice[54] have shown that PPARα protects from steatosis[19,54]. Moreover, several clinical lines of evidence indicate that PPARα is also influential in human NASH[55].

Most studies performed *in vivo* in *Pparα*-null mice have suggested that the mechanisms by which PPARα protects from steatosis and NASH involve its ability to transactivate genes required for fatty acid catabolism[38] and to repress a number of inflammatory genes[39,41]. Because PPARα is expressed in many cell types and tissues with high fatty acid oxidation activity[29–31,34], it is interesting to define *in vivo* the specific contribution of hepatocytic PPARα in preventing NAFLD.

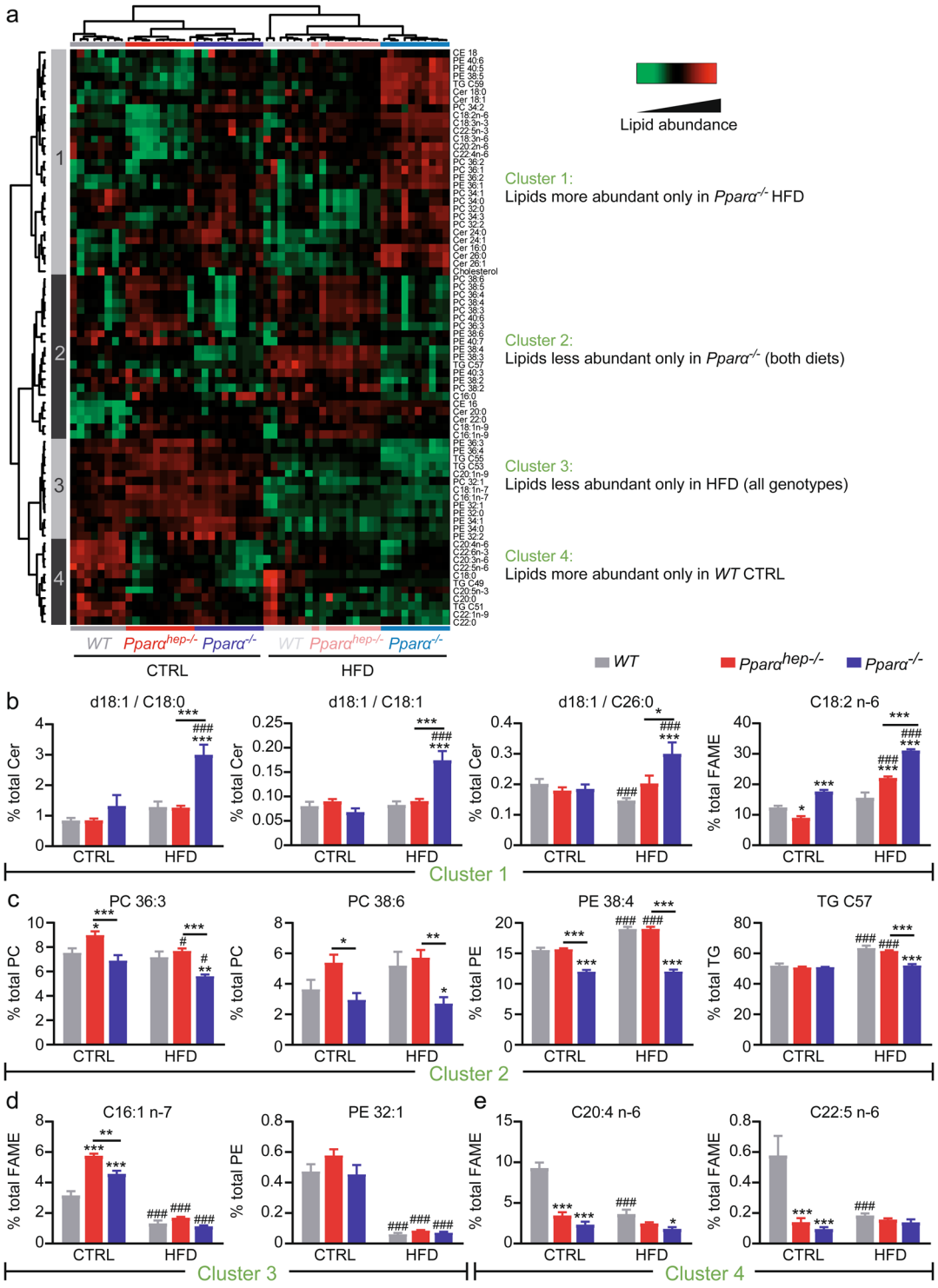

Figure 7. PPARα-dependent regulation of hepatic lipid homeostasis in response to HFD. *WT*, *Pparα*$^{hep-/-}$, and *Pparα*$^{-/-}$ mice were fed a control diet (CTRL) or a HFD for 10 weeks at 30 °C (thermoneutrality). (**a**) Heat map of data from hepatic lipid profiling in *WT*, *Pparα*$^{hep-/-}$, and *Pparα*$^{-/-}$ mice exposed to HFD. Hierarchical clustering is also shown and defines four main lipid clusters. Representation of characteristic lipid species defining cluster 1 (**b**), 2 (**c**), 3 (**d**), and 4 (**e**). Data represent mean ± SEM. #, significant diet effect and *, significant genotype effect. $^{\#}$ or *$p \leq 0.05$; $^{\#\#}$ or **$p \leq 0.01$; $^{\#\#\#}$ or ***$p \leq 0.001$. Cer: ceramide; SM: sphingomyelin; TG: triglyceride; PC: phosphatidyl choline; PE: phosphatidyl ethanolamine; CE: cholesterol ester.

When fed a regular diet, *Pparα*$^{-/-}$ mice are steatotic and overweight as previously reported[26,38]. When fed a HFD, they become even more steatotic and develop further liver inflammation[39,41]. Importantly, although *Pparα*-null mice develop steatosis, they do not exhibit reduced glucose tolerance compared to *WT* mice[43]. The data we obtained in *Pparα*$^{hep-/-}$ mice fed a HFD indicate that the deletion of *Pparα* in hepatocytes is sufficient to promote steatosis and inflammation. Therefore, hepatocyte-specific *Pparα* deletion promotes steatosis and liver inflammation while dissociating steatosis from glucose intolerance as observed in *Pparα*$^{-/-}$ mice[42,43].

The mechanisms involved in the susceptibility to steatosis and protection from glucose intolerance likely involve the well-established role of PPARα in the control of fatty acid transport and degradation[18]. The mechanisms by which hepatocyte *Pparα* deficiency promotes NASH likely involve lipotoxic fat accumulation, including linoleic acid (C18:2n-6), which was recently identified as promoting NAFLD etiology *in vivo*[56]. Moreover, we extend previous observations and confirm the role of hepatocyte PPARα in repressing the expression of inflammatory genes, such as those involved in the NF-kappa B pathway[57,58]. However, by comparing the HFD response in *Pparα*$^{-/-}$ and in *Pparα*$^{hep-/-}$ mice we observed differences in the expression of genes involved in inflammation (cell morphology, adhesion and migration) strongly suggesting that PPARα activity might be important for liver immune cells activity in the context of obesity.

This study not only shows a specific effect of hepatocyte PPARα activity, but also identifies several roles of non-hepatocytic PPARα. First, we confirmed our previous observations that, unlike *Pparα*$^{hep-/-}$ mice, *Pparα*$^{-/-}$ mice gain weight when fed a regular diet[19]. Moreover, because the current observations were made at thermoneutrality, this weight gain is not likely due to defective PPARα expression and activity in the brown adipose tissue. In addition, by combining different large or medium scale analyses of the liver transcriptome and metabolome, we showed that the response to HFD was different in *Pparα*$^{-/-}$ mice compared to *Pparα*$^{hep-/-}$ mice, showing that extra-hepatocyte PPARα mediates at least a part of the adaptive response to HFD. Since we observed significant differences in lipid metabolism between *Pparα*$^{-/-}$ and *Pparα*$^{hep-/-}$ mice fed a HFD, our results are consistent with a possible extra-hepatic influence of PPARα on whole body fatty acid and cholesterol homeostasis.

Taken together, our data demonstrate that hepatocyte-specific deletion of *Pparα* promotes steatosis and inflammation in HFD-induced obesity and provide further pre-clinical evidence that hepatocyte PPARα is a relevant direct target in NAFLD. Our data also suggest that extra-hepatic PPARα plays a major homeostatic role in the control of the metabolic response to HFD. These data are in agreement with a recent study providing evidence that extrahepatic PPARα activity such as in skeletal muscle and heart, may contribute to whole body fatty acid homeostasis[59]. Further research is required to investigate in which cells, other than hepatocytes, PPARα regulates lipid metabolism in health and disease.

Material and Methods

Mice. All experiments were approved by the relevant animal care and use committee (CEEA-86, Ministry of Research and Higher Education, France); notification TOXCOM108, and conducted in accordance with the European directive 2010/63/UE.

Pparα$^{hep-/-}$ animals were created at INRA's rodent facility (Toulouse, France) by mating the floxed-*Pparα* mouse strain with C57BL/6 J albumin-Cre transgenic mice (a gift from Prof. Didier Trono, EPFL, Lausanne, Switzerland) to obtain albumin-Cre$^{+/-}$*Pparα*$^{flox/flox}$ mice (i.e., *Pparα*$^{hep-/-}$ mice as described in[19]). The *Pparα* deletion was confirmed with PCR and HotStar Taq DNA Polymerase (5 U/µl, Qiagen) using the following primers: forward: 5′- AAAGCAGCCAGCTCTGTGTTGAGC-3′ and reverse, 5′-TAGGTACCGTGGACTCAGAGCTAG-3′. The amplification conditions were as follows: 95 °C for 15 min, followed by 35 cycles of 94 °C for 1 min, 65 °C for 1 min, and 72 °C for 1 min, and a final cycle of 72 °C for 10 min. This reaction produced 450-bp, 915-bp, and 1070-bp fragments, which represented the *Pparα* sequence with an exon 4 deletion, the wild-type allele, and the floxed allele, respectively. The albumin-Cre allele was detected by PCR using the following primer pairs: CreU, 5′-AGGTGTAGAGAAGGCACTTAG-3′ and CreD, 5′- CTAATCGCCATCTTCCAGCAGG-3′; G2lox7F, 5′-CCAATCCCTTGGTTCATGGTTGC- 3′ and G2lox7R, 5′-CGTAAGGCCCAAGGAAGTCCTGC-3′).

Pparα-deficient C57BL/6 J mice (*Pparα*$^{-/-}$) were bred at INRA's transgenic rodent facility. Age-matched C57BL/6 J (provided by Charles River) were acclimated for 2 weeks to the local animal facility conditions prior to the experiment.

Mouse housing was controlled for temperature and light (12-h light/12-h dark). All mice were placed in a ventilated cabinet at the specific temperature of 30 °C (thermoneutrality) throughout the experiment. All animals used in these experiments were male mice.

Diet. *WT*, *Pparα*$^{-/-}$ and *Pparα*$^{hep-/-}$ mice were fed a standard diet (Safe 04 U8220G10R) until 8 weeks old, when the mice were fed a high fat diet (D12492, Research Diet) thought to induce mild hepatic lesions[60]. This HFD contains 60% calories from fat (lard), 20% calories from carbohydrates (7% sucrose) and 20% calories from proteins; or a chow diet (D12450J, Research Diet) containing 10% calories from fat, 70% calories from carbohydrates (7% sucrose) and 20% calories from protein during 10 weeks (until 20 weeks old). The estimated cholesterol content is: 0.014 g/kg (chow diet) and 0.228 g/kg (HFD diet). Experimental groups were designed as follows: *WT* CTRL, 8 mice; WT HFD, 8 mice; *Pparα*$^{hep-/-}$ CTRL, 10 mice; *Pparα*$^{hep-/-}$ HFD, 9 mice; *Pparα*$^{-/-}$ CTRL, 10 mice; *Pparα*$^{-/-}$ HFD, 10 mice.

Oral glucose tolerance test. Mice were fasted for 6 h and received an oral (2 g/kg body weight) glucose load. Blood glucose was measured at the tail vein using an AccuCheck Performa glucometer (Roche Diagnostics) at −15, 0, 15, 30, 45, 60, 90, and 120 minutes.

Blood and tissue samples. Prior to sacrifice, blood was collected in EDTA-coated tubes (BD Microtainer, K2E tubes) from the submandibular vein. All mice were killed in a fed state. Plasma was collected by

centrifugation (1500 × g, 10 min, 4 °C) and stored at −80 °C. Following killing by cervical dislocation, the organs were removed, weighted, dissected and used for histological analysis or snap-frozen in liquid nitrogen and stored at −80 °C.

Gene expression. Total cellular RNA was extracted with Tri reagent (Molecular Research Center). Total RNA samples (2 µg) were then reverse-transcribed with the High-capacity cDNA Reverse Transcription Kit (Applied Biosystems) for real-time quantitative polymerase chain reaction (qPCR) analyses. The primers for Sybr Green assays are presented in Supplementary Table 1. Amplifications were performed on a Stratagene Mx3005P (Agilent Technology). The qPCR data were normalized to the level of the TATA-box binding protein (TBP) messenger RNA (mRNA) and analysed by the LinRegPCR v.11 software[61].

Gene expression profiles were performed at the GeT-TRiX facility (GénoToul, Génopole Toulouse Midi-Pyrénées) using Agilent Sureprint G3 Mouse microarrays (8 × 60 K, design 077809) following the manufacturer's instructions. For each sample, Cyanine-3 (Cy3) labeled cRNA was prepared from 200 ng of total RNA using the One-Color Quick Amp Labeling kit (Agilent) according to the manufacturer's instructions, followed by Agencourt RNAClean XP (Agencourt Bioscience Corporation, Beverly, Massachusetts). Dye incorporation and cRNA yield were checked using Dropsense™ 96 UV/VIS droplet reader (Trinean, Belgium). 600 ng of Cy3-labelled cRNA were hybridized on the microarray slides following the manufacturer's instructions. Immediately after washing, the slides were scanned on Agilent G2505C Microarray Scanner using Agilent Scan Control A.8.5.1 software and fluorescence signal extracted using Agilent Feature Extraction software v10.10.1.1 with default parameters.

Microarray data and experimental details are available in NCBI's Gene Expression Omnibus[62] and are accessible through GEO Series accession number GSE123354 (https://www.ncbi.nlm.nih.gov/geo/query/acc.cgi?acc=GSE123354).

Histology. Formalin-fixed, paraffin-embedded liver tissue was sliced into 3 µm sections and stained with haematoxylin and eosin (H&E) for histopathological analysis. The staining was visualized with a Leica microscope DM4000 B equipped with a Leica DFC450 C camera. The H&E-stained livers sections were analysed blindly for the steatosis and the inflammation (NAFLD activity score or NAS) according to Kleiner *et al.*[49], Steatosis was measured depending on i) the percentage of liver cells containing fat (Grade 0 to 3); ii) the localisation of steatosis (Grade 0 to 3); and iii) the presence of microvesicular steatosis (Grade 0 to 1). The degree of inflammation was appreciated by counting the inflammatory foci into 10 distinct area at 200X for each liver slice (Grade 0 to 3). Values represent the mean of 10 fields/liver slice.

Biochemical analysis. Aspartate transaminase (AST), alanine transaminase (ALT), total cholesterol, LDL and HDL cholesterols were determined from plasma samples using a COBASMIRA + biochemical analyser (Anexplo facility).

Analysis of liver neutral lipids. Lipids were analysed as previously described[20]. Tissue samples were homogenized in methanol/5 mM EGTA (2:1, v/v), and lipids (corresponding to an equivalent of 2 mg tissue) extracted according to the Bligh–Dyer method[63], with chloroform/methanol/water (2.5:2.5:2 v/v/v), in the presence of the following internal standards: glyceryl trinonadecanoate, stigmasterol, and cholesteryl heptadecanoate (Sigma). Triglycerides, free cholesterol, and cholesterol esters were analysed by gas-liquid chromatography on a Focus Thermo Electron system equipped with a Zebron- 1 Phenomenex fused-silica capillary column (5 m, 0.25 mm i.d., 0.25 mm film thickness). The oven temperature was programmed to increase from 200 to 350 °C at 5 °C/min, and the carrier gas was hydrogen (0.5 bar). The injector and detector temperatures were 315 °C and 345 °C, respectively.

Liver fatty acid analysis. To measure all hepatic fatty acid methyl ester (FAME) molecular species, lipids that corresponded to an equivalent of 1 mg of liver were extracted in the presence of the internal standard, glyceryl triheptadecanoate (2 µg). The lipid extract was transmethylated with 1 ml BF3 in methanol (14% solution; Sigma) and 1 ml heptane for 60 min at 80 °C, and evaporated to dryness. The FAMEs were extracted with heptane/water (2:1). The organic phase was evaporated to dryness and dissolved in 50 µl ethyl acetate. A sample (1 µl) of total FAME was analysed by gas-liquid chromatography (Clarus 600 Perkin Elmer system, with Famewax RESTEK fused silica capillary columns, 30-m × 0.32-mm i.d., 0.25-µm film thickness). The oven temperature was programmed to increase from 110 °C to 220 °C at a rate of 2 °C/min, and the carrier gas was hydrogen (7.25 psi). The injector and detector temperatures were 225 °C and 245 °C, respectively.

Liver phospholipid and sphingolipid analysis. *Chemicals and reagents.* The liquid chromatography solvent, acetonitrile, was HPLC-grade and purchased from Acros Organics. Ammonium formate (>99%) was supplied by Sigma Aldrich. Synthetic lipid standards (Cer d18:1/18:0, Cer d18:1/15:0, PE 12:0/12:0, PE 16:0/16:0, PC 13:0/13:0, PC 16:0/16:0, SM d18:1/18:0, SM d18:1/12:0) were purchased from Avanti Polar Lipids.

Lipid extraction. Lipids were extracted from the liver (1 mg) as described by Bligh and Dyer in dichloromethane / methanol (2% acetic acid) / water (2.5:2.5:2 v/v/v). Internal standards were added (Cer d18:1/15:0, 16 ng; PE 12:0/12:0, 180 ng; PC 13:0/13:0, 16 ng; SM d18:1/12:0, 16 ng; PI 16:0/17:0, 30 ng; PS 12:0/12:0, 156.25 ng). The solution was centrifuged at 1500 rpm for 3 min. The organic phase was collected and dried under azote, then dissolved in 50 µl MeOH. Sample solutions were analysed using an Agilent 1290 UPLC system coupled to a G6460 triple quadripole spectrometer (Agilent Technologies). MassHunter software was used for data acquisition and analysis. A Kinetex HILIC column (Phenomenex, 50 × 4.6 mm, 2.6 µm) was used for LC separations. The column temperature was maintained at 40 °C. Mobile phase A was acetonitrile and B was 10 mM ammonium formate in

water at pH 3.2. The gradient was as follows: from 10% to 30% B in 10 min, 100% B from 10 to 12 min, and then back to 10% B at 13 min for 1 min to re-equilibrate prior to the next injection. The flow rate of the mobile phase was 0.3 ml/min, and the injection volume was 5 µl. An electrospray source was employed in positive (for Cer, PE, PC, and SM analysis) or negative ion mode (for PI and PS analysis). The collision gas was nitrogen. Needle voltage was set at +4000 V. Several scan modes were used. First, to obtain the naturally different masses of different species, we analysed cell lipid extracts with a precursor ion scan at 184 m/z, 241 m/z, and 264 m/z for PC/SM, PI, and Cer, respectively. We performed a neutral loss scan at 141 and 87 m/z for PE and PS, respectively. The collision energy optimums for Cer, PE, PC, SM, PI, and PS were 25 eV, 20 eV, 30 eV, 25 eV, 45 eV, and 22 eV, respectively. The corresponding SRM transitions were used to quantify different phospholipid species for each class. Two MRM acquisitions were necessary, due to important differences between phospholipid classes. Data were treated with QqQ Quantitative (vB.05.00) and Qualitative analysis software (vB.04.00).

Metabolomic analyses by 1H nuclear magnetic resonance (NMR) spectroscopy. ^{1}H NMR spectroscopy was performed on aqueous liver extracts prepared from liver samples (50–75 mg) homogenized in chloroform/methanol/NaCl 0.9% (2/1/0.6) containing 0.1% butyl hydroxytoluene and centrifuged at 5000 × g for 10 min. The supernatant was collected, lyophilized, and reconstituted in 600 µl of D2O containing 0.25 mM TSP [3-(trimethylsilyl)propionic-(2,2,3,3-d4) acid sodium salt] as a chemical shift reference at 0 ppm. All 1 H NMR spectra were obtained on a Bruker DRX-600 Avance NMR spectrometer operating at 600.13 MHz for 1 H resonance frequency using an inverse detection 5 mm 1H-13C-15N cryoprobe attached to a CryoPlatform (the preamplifier cooling unit). The 1 H NMR spectra were acquired at 300 K with a 1D NOESY-presat sequence (relaxation delay – 90°-t-90°-tm-90°-acquisition). A total of 128 transients were acquired into a spectrum with 20 ppm width, 32 k data points, a relaxation delay of 2.0 s, and a mixing delay of 100 ms. All 1 H spectra were zero-filled to 64 k points and subjected to 0.3 Hz exponential line broadening before Fourier transformation. The spectra were phase and baseline corrected and referenced to TSP (1 H, d 0.0 ppm) using Bruker Topspin 2.1 software (Bruker GmbH, Karlsruhe, Germany). Multivariate analysis of metabolomic data was performed.

Statistical analysis. Biochemical, qPCR and phenotypic data were analysed using and graphpad software. Differential effects were assessed on log2 transformed data by performing ANOVA followed by Sidak post-hoc tests. p-values < 0.05 were considered significant.

Hierarchical clustering of lipid quantification data was performed using R (R Development Core Team, 2018) with the heatmap.2 function from the package, gplots. Data were log2 transformed, then centred and scaled by lipid. Hierarchical clustering was applied to the samples and the lipids using 1-Pearson correlation coefficient as distance and Ward's criterion (Ward.D2) for agglomeration. All the data represented on the heat map had adjusted p-values <0.05 for one or more comparisons performed with an analysis of variance.

Microarray data were analyzed using R and Bioconductor packages (www.bioconductor.org, v 3.0), as described in GEO accession GSE123354. Raw data (median signal intensity) were filtered, log2 transformed, corrected for batch effects (microarray washing bath) and normalized using quantile method[64].

A model was fitted using the limma lmFit function[65] considering array weights using arrayWeights function. Pair-wise comparisons between biological conditions were applied using specific contrasts. A correction for multiple testing was applied using Benjamini-Hochberg procedure[66] for False Discovery Rate (FDR). Probes with FDR ≤ 0.05 were considered to be differentially expressed between conditions.

In addition to the differential analysis, a multivariate exploratory analysis was performed. A Sparse Partial Least Squares Discriminant Analysis[67] (sPLS-DA) was conducted using mixOmics package[68] under to select the most discriminative variables (genes) that help classify the samples according to their experimental conditions among their expression values. Twenty iterations of 5-fold cross-validation was used to evaluate the model performance for the selection of the most informative components (6 components chosen) using all the variables (PLS-DA). Then a "sparse" PLS-DA model was parametrized selecting the first 100, 120, 80, 40, 100 and 20 (chosen according the performance results of 20 iterations of 5-fold cross-validations) most discriminant variables on the components 1 to 6 respectively.

Hierarchical clustering was applied to the samples and the differentially expressed probes using 1-Pearson correlation coefficient as distance and Ward's criterion for agglomeration. The clustering results are illustrated as a heatmap of expression signals. Gene network and enrichment of KEGG pathways was either performed using the online software STRING V.11[69] or Metascape[70]. Correlation graphic chart was generated using the chart correlation function from the Performance Analytics package.

Received: 6 February 2019; Accepted: 30 March 2020;
Published online: 16 April 2020

References

1. Younossi, Z. M. *et al*. Global epidemiology of nonalcoholic fatty liver disease-Meta-analytic assessment of prevalence, incidence, and outcomes. *Hepatology* **64**, 73–84, https://doi.org/10.1002/hep.28431 (2016).
2. Samuel, V. T. & Shulman, G. I. Nonalcoholic Fatty Liver Disease as a Nexus of Metabolic and Hepatic Diseases. *Cell Metab* **27**, 22–41, https://doi.org/10.1016/j.cmet.2017.08.002 (2018).
3. Donnelly, K. L. *et al*. Sources of fatty acids stored in liver and secreted via lipoproteins in patients with nonalcoholic fatty liver disease. *J Clin Invest* **115**, 1343–1351, https://doi.org/10.1172/jci23621 (2005).
4. Hernández, E. Á. *et al*. Acute dietary fat intake initiates alterations in energy metabolism and insulin resistance. *The Journal of clinical investigation* **127**, 695–708, https://doi.org/10.1172/JCI89444 (2017).
5. Tamura, S. & Shimomura, I. Contribution of adipose tissue and de novo lipogenesis to nonalcoholic fatty liver disease. *J Clin Invest* **115**, 1139–1142, https://doi.org/10.1172/jci24930 (2005).

6. Marra, F., Gastaldelli, A., Svegliati Baroni, G., Tell, G. & Tiribelli, C. Molecular basis and mechanisms of progression of non-alcoholic steatohepatitis. *Trends Mol Med* **14**, 72–81, https://doi.org/10.1016/j.molmed.2007.12.003 (2008).
7. Hebbard, L. & George, J. Animal models of nonalcoholic fatty liver disease. *Nat Rev Gastroenterol Hepatol* **8**, 35–44, https://doi.org/10.1038/nrgastro.2010.191 (2011).
8. Rotman, Y. & Sanyal, A. J. Current and upcoming pharmacotherapy for non-alcoholic fatty liver disease. *Gut* **66**, 180–190, https://doi.org/10.1136/gutjnl-2016-312431 (2017).
9. Wong, V. W., Adams, L. A., de Ledinghen, V., Wong, G. L. & Sookoian, S. Noninvasive biomarkers in NAFLD and NASH - current progress and future promise. *Nat Rev Gastroenterol Hepatol* **15**, 461–478, https://doi.org/10.1038/s41575-018-0014-9 (2018).
10. Gross, B., Pawlak, M., Lefebvre, P. & Staels, B. PPARs in obesity-induced T2DM, dyslipidaemia and NAFLD. *Nat Rev Endocrinol* **13**, 36–49, https://doi.org/10.1038/nrendo.2016.135 (2017).
11. Krey, G. *et al.* Fatty acids, eicosanoids, and hypolipidemic agents identified as ligands of peroxisome proliferator-activated receptors by coactivator-dependent receptor ligand assay. *Mol Endocrinol* **11**, 779–791, https://doi.org/10.1210/mend.11.6.0007 (1997).
12. Devchand, P. R. *et al.* The PPARalpha-leukotriene B4 pathway to inflammation control. *Nature* **384**, 39–43, https://doi.org/10.1038/384039a0 (1996).
13. Chakravarthy, M. V. *et al.* Identification of a physiologically relevant endogenous ligand for PPARalpha in liver. *Cell* **138**, 476–488, https://doi.org/10.1016/j.cell.2009.05.036 (2009).
14. Dubois, V., Eeckhoute, J., Lefebvre, P. & Staels, B. Distinct but complementary contributions of PPAR isotypes to energy homeostasis. *J Clin Invest* **127**, 1202–1214, https://doi.org/10.1172/jci88894 (2017).
15. Ip, E., Farrell, G., Hall, P., Robertson, G. & Leclercq, I. Administration of the potent PPARalpha agonist, Wy-14,643, reverses nutritional fibrosis and steatohepatitis in mice. *Hepatology* **39**, 1286–1296, https://doi.org/10.1002/hep.20170 (2004).
16. Staels, B. *et al.* Hepatoprotective effects of the dual peroxisome proliferator-activated receptor alpha/delta agonist, GFT505, in rodent models of nonalcoholic fatty liver disease/nonalcoholic steatohepatitis. *Hepatology* **58**, 1941–1952, https://doi.org/10.1002/hep.26461 (2013).
17. Braissant, O., Foufelle, F., Scotto, C., Dauca, M. & Wahli, W. Differential expression of peroxisome proliferator-activated receptors (PPARs): tissue distribution of PPAR-alpha, -beta, and -gamma in the adult rat. *Endocrinology* **137**, 354–366, https://doi.org/10.1210/endo.137.1.8536636 (1996).
18. Kersten, S. Integrated physiology and systems biology of PPARalpha. *Mol Metab* **3**, 354–371, https://doi.org/10.1016/j.molmet.2014.02.002 (2014).
19. Montagner, A. *et al.* Liver PPARalpha is crucial for whole-body fatty acid homeostasis and is protective against NAFLD. *Gut* **65**, 1202–1214, https://doi.org/10.1136/gutjnl-2015-310798 (2016).
20. Regnier, M. *et al.* Insights into the role of hepatocyte PPARalpha activity in response to fasting. *Mol Cell Endocrinol* **471**, 75–88, https://doi.org/10.1016/j.mce.2017.07.035 (2018).
21. Goldstein, I. & Hager, G. L. Transcriptional and Chromatin Regulation during Fasting - The Genomic Era. *Trends Endocrinol Metab* **26**, 699–710, https://doi.org/10.1016/j.tem.2015.09.005 (2015).
22. Hondares, E. *et al.* Hepatic FGF21 expression is induced at birth via PPARalpha in response to milk intake and contributes to thermogenic activation of neonatal brown fat. *Cell Metab* **11**, 206–212, https://doi.org/10.1016/j.cmet.2010.02.001 (2010).
23. Cotter, D. G., Ercal, B., d'Avignon, D. A., Dietzen, D. J. & Crawford, P. A. Impairments of hepatic gluconeogenesis and ketogenesis in PPARalpha- deficient neonatal mice. *Am J Physiol Endocrinol Metab* **307**, E176–185, https://doi.org/10.1152/ajpendo.00087.2014 (2014).
24. Rando, G. *et al.* Glucocorticoid receptor-PPARalpha axis in fetal mouse liver prepares neonates for milk lipid catabolism. *Elife* **5**, https://doi.org/10.7554/eLife.11853 (2016).
25. Kersten, S. *et al.* Peroxisome proliferator-activated receptor alpha mediates the adaptive response to fasting. *J Clin Invest* **103**, 1489–1498, https://doi.org/10.1172/jci6223 (1999).
26. Kroetz, D. L., Yook, P., Costet, P., Bianchi, P. & Pineau, T. Peroxisome proliferator-activated receptor alpha controls the hepatic CYP4A induction adaptive response to starvation and diabetes. *J Biol Chem* **273**, 31581–31589, https://doi.org/10.1074/jbc.273.47.31581 (1998).
27. Leone, T. C., Weinheimer, C. J. & Kelly, D. P. A critical role for the peroxisome proliferator-activated receptor alpha (PPARalpha) in the cellular fasting response: the PPARalpha-null mouse as a model of fatty acid oxidation disorders. *Proc Natl Acad Sci USA* **96**, 7473–7478, https://doi.org/10.1073/pnas.96.13.7473 (1999).
28. Polizzi, A. *et al.* Hepatic Fasting-Induced PPARalpha Activity Does Not Depend on Essential Fatty Acids. *Int J Mol Sci* **17**, https://doi.org/10.3390/ijms17101624 (2016).
29. Liu, S. *et al.* A diurnal serum lipid integrates hepatic lipogenesis and peripheral fatty acid use. *Nature* **502**, 550–554, https://doi.org/10.1038/nature12710 (2013).
30. Tsuchida, A. *et al.* Peroxisome proliferator-activated receptor (PPAR)alpha activation increases adiponectin receptors and reduces obesity-related inflammation in adipose tissue: comparison of activation of PPARalpha, PPARgamma, and their combination. *Diabetes* **54**, 3358–3370, https://doi.org/10.2337/diabetes.54.12.3358 (2005).
31. Goto, T. *et al.* Activation of peroxisome proliferator-activated receptor-alpha stimulates both differentiation and fatty acid oxidation in adipocytes. *J Lipid Res* **52**, 873–884, https://doi.org/10.1194/jlr.M011320 (2011).
32. Barquissau, V. *et al.* White-to-brite conversion in human adipocytes promotes metabolic reprogramming towards fatty acid anabolic and catabolic pathways. *Mol Metab* **5**, 352–365, https://doi.org/10.1016/j.molmet.2016.03.002 (2016).
33. Defour, M. *et al.* The Peroxisome Proliferator-Activated Receptor alpha is dispensable for cold-induced adipose tissue browning in mice. *Mol Metab* **10**, 39–54, https://doi.org/10.1016/j.molmet.2018.01.023 (2018).
34. Bunger, M. *et al.* Genome-wide analysis of PPARalpha activation in murine small intestine. *Physiol Genomics* **30**, 192–204, https://doi.org/10.1152/physiolgenomics.00198.2006 (2007).
35. Haemmerle, G. *et al.* ATGL-mediated fat catabolism regulates cardiac mitochondrial function via PPAR-alpha and PGC-1. *Nat Med* **17**, 1076–1085, https://doi.org/10.1038/nm.2439 (2011).
36. Sugden, M. C., Bulmer, K., Gibbons, G. F. & Holness, M. J. Role of peroxisome proliferator-activated receptor-alpha in the mechanism underlying changes in renal pyruvate dehydrogenase kinase isoform 4 protein expression in starvation and after refeeding. *Arch Biochem Biophys* **395**, 246–252, https://doi.org/10.1006/abbi.2001.2586 (2001).
37. Costet, P. *et al.* Peroxisome proliferator-activated receptor alpha-isoform deficiency leads to progressive dyslipidemia with sexually dimorphic obesity and steatosis. *J Biol Chem* **273**, 29577–29585, https://doi.org/10.1074/jbc.273.45.29577 (1998).
38. Abdelmegeed, M. A. *et al.* PPARalpha expression protects male mice from high fat-induced nonalcoholic fatty liver. *J Nutr* **141**, 603–610, https://doi.org/10.3945/jn.110.135210 (2011).
39. Patsouris, D., Reddy, J. K., Muller, M. & Kersten, S. Peroxisome proliferator-activated receptor alpha mediates the effects of high-fat diet on hepatic gene expression. *Endocrinology* **147**, 1508–1516, https://doi.org/10.1210/en.2005-1132 (2006).
40. Stienstra, R. *et al.* Peroxisome proliferator-activated receptor alpha protects against obesity-induced hepatic inflammation. *Endocrinology* **148**, 2753–2763, https://doi.org/10.1210/en.2007-0014 (2007).
41. Ip, E. *et al.* Central role of PPARalpha-dependent hepatic lipid turnover in dietary steatohepatitis in mice. *Hepatology* **38**, 123–132, https://doi.org/10.1053/jhep.2003.50307 (2003).
42. Guerre-Millo, M. *et al.* PPAR-alpha-null mice are protected from high-fat diet-induced insulin resistance. *Diabetes* **50**, 2809–2814, https://doi.org/10.2337/diabetes.50.12.2809 (2001).

43. Patsouris, D. *et al*. PPARalpha governs glycerol metabolism. *J Clin Invest* **114**, 94–103, https://doi.org/10.1172/jci20468 (2004).
44. Badman, M. K. *et al*. Hepatic fibroblast growth factor 21 is regulated by PPARalpha and is a key mediator of hepatic lipid metabolism in ketotic states. *Cell Metab* **5**, 426–437, https://doi.org/10.1016/j.cmet.2007.05.002 (2007).
45. Iroz, A. *et al*. A Specific ChREBP and PPARalpha Cross-Talk Is Required for the Glucose- Mediated FGF21 Response. *Cell Rep* **21**, 403–416, https://doi.org/10.1016/j.celrep.2017.09.065 (2017).
46. Kharitonenkov, A. & DiMarchi, R. FGF21 Revolutions: Recent Advances Illuminating FGF21 Biology and Medicinal Properties. *Trends Endocrinol Metab* **26**, 608–617, https://doi.org/10.1016/j.tem.2015.09.007 (2015).
47. Fisher, F. M. *et al*. Fibroblast growth factor 21 limits lipotoxicity by promoting hepatic fatty acid activation in mice on methionine and choline-deficient diets. *Gastroenterology* **147**, 1073–1083.e1076, https://doi.org/10.1053/j.gastro.2014.07.044 (2014).
48. Singhal, G. *et al*. Deficiency of fibroblast growth factor 21 (FGF21) promotes hepatocellular carcinoma (HCC) in mice on a long term obesogenic diet. *Mol Metab* **13**, 56–66, https://doi.org/10.1016/j.molmet.2018.03.002 (2018).
49. Kleiner, D. E. *et al*. Design and validation of a histological scoring system for nonalcoholic fatty liver disease. *Hepatology* **41**, 1313–1321, https://doi.org/10.1002/hep.20701 (2005).
50. van Diepen, J. A. *et al*. PPAR-alpha dependent regulation of vanin-1 mediates hepatic lipid metabolism. *J Hepatol* **61**, 366–372, https://doi.org/10.1016/j.jhep.2014.04.013 (2014).
51. Estes, C., Razavi, H., Loomba, R., Younossi, Z. & Sanyal, A. J. Modeling the epidemic of nonalcoholic fatty liver disease demonstrates an exponential increase in burden of disease. *Hepatology* **67**, 123–133, https://doi.org/10.1002/hep.29466 (2018).
52. Wettstein, G. *et al*. The new-generation pan-peroxisome proliferator-activated receptor agonist IVA337 protects the liver from metabolic disorders and fibrosis. *Hepatol Commun* **1**, 524–537, https://doi.org/10.1002/hep4.1057 (2017).
53. Ratziu, V. *et al*. Elafibranor, an Agonist of the Peroxisome Proliferator-Activated Receptor-alpha and -delta, Induces Resolution of Nonalcoholic Steatohepatitis Without Fibrosis Worsening. *Gastroenterology* **150**, 1147–1159.e1145, https://doi.org/10.1053/j.gastro.2016.01.038 (2016).
54. Lee, S. S. *et al*. Targeted disruption of the alpha isoform of the peroxisome proliferator- activated receptor gene in mice results in abolishment of the pleiotropic effects of peroxisome proliferators. *Mol Cell Biol* **15**, 3012–3022, https://doi.org/10.1128/mcb.15.6.3012 (1995).
55. Francque, S. *et al*. PPARalpha gene expression correlates with severity and histological treatment response in patients with non-alcoholic steatohepatitis. *J Hepatol* **63**, 164–173, https://doi.org/10.1016/j.jhep.2015.02.019 (2015).
56. Ma, C. *et al*. NAFLD causes selective CD4(+) T lymphocyte loss and promotes hepatocarcinogenesis. *Nature* **531**, 253–257, https://doi.org/10.1038/nature16969 (2016).
57. Mansouri, R. M., Bauge, E., Staels, B. & Gervois, P. Systemic and distal repercussions of liver-specific peroxisome proliferator-activated receptor-alpha control of the acute-phase response. *Endocrinology* **149**, 3215–3223, https://doi.org/10.1210/en.2007-1339 (2008).
58. Pawlak, M., Lefebvre, P. & Staels, B. Molecular mechanism of PPARalpha action and its impact on lipid metabolism, inflammation and fibrosis in non-alcoholic fatty liver disease. *J Hepatol* **62**, 720–733, https://doi.org/10.1016/j.jhep.2014.10.039 (2015).
59. Brocker, C. N. *et al*. Extrahepatic PPARalpha modulates fatty acid oxidation and attenuates fasting-induced hepatosteatosis in mice. *J Lipid Res* **59**, 2140–2152, https://doi.org/10.1194/jlr.M088419 (2018).
60. Farrell, G. *et al*. Mouse Models of Nonalcoholic Steatohepatitis: Toward Optimization of Their Relevance to Human Nonalcoholic Steatohepatitis. *Hepatology (Baltimore, Md.)* **69**, 2241–2257, https://doi.org/10.1002/hep.30333 (2019).
61. Ruijter, J. M. *et al*. Amplification efficiency: linking baseline and bias in the analysis of quantitative PCR data. *Nucleic Acids Res* **37**, e45, https://doi.org/10.1093/nar/gkp045 (2009).
62. Edgar, R., Domrachev, M. & Lash, A. E. Gene Expression Omnibus: NCBI gene expression and hybridization array data repository. *Nucleic Acids Res* **30**, 207–210, https://doi.org/10.1093/nar/30.1.207 (2002).
63. Bligh, E. G. & Dyer, W. J. A rapid method of total lipid extraction and purification. *Can J Biochem Physiol* **37**, 911–917, https://doi.org/10.1139/o59-099 (1959).
64. Bolstad, B. M., Irizarry, R. A., Astrand, M. & Speed, T. P. A comparison of normalization methods for high density oligonucleotide array data based on variance and bias. *Bioinformatics* **19**, 185–193, https://doi.org/10.1093/bioinformatics/19.2.185 (2003).
65. Ritchie, M. E. *et al*. limma powers differential expression analyses for RNA-sequencing and microarray studies. *Nucleic Acids Res* **43**, e47, https://doi.org/10.1093/nar/gkv007 (2015).
66. Benjamini, Y. & Hochberg, Y. Controlling the False Discovery Rate: A Practical and Powerful Approach to Multiple Testing. *Royal statistical society* **57**, 289–300 (1995).
67. Le Cao, K. A., Boitard, S. & Besse, P. Sparse PLS discriminant analysis: biologically relevant feature selection and graphical displays for multiclass problems. *BMC Bioinformatics* **12**, 253, https://doi.org/10.1186/1471-2105-12-253 (2011).
68. Le Cao, K. A. *et al*. MixMC: A Multivariate Statistical Framework to Gain Insight into Microbial Communities. *PLoS One* **11**, e0160169, https://doi.org/10.1371/journal.pone.0160169 (2016).
69. Szklarczyk, D. *et al*. STRING v10: protein-protein interaction networks, integrated over the tree of life. *Nucleic Acids Res* **43**, D447–452, https://doi.org/10.1093/nar/gku1003 (2015).
70. Zhou, Y. *et al*. Metascape provides a biologist-oriented resource for the analysis of systems-level datasets. *Nat Commun* **10**, 1523–1523, https://doi.org/10.1038/s41467-019-09234-6 (2019).

Acknowledgements

We thank all members of the EZOP staff for their careful help from the early start of this project. We thank Léa Morra-Charrot and Laurent Monbrun from Anexplo for their excellent work on plasma biochemistry. We thank the staff from the Genotoul: Anexplo, GeT-TRiX and Metatoul-Lipidomic facilities. The authors wish to thank Pr Daniel Metzger, Pr Pierre Chambon (IGBMC, Illkirch, France) and the staff of the Mouse Clinical Institute (Illkirch, France) for their critical support in this project. We thank Pr Didier Trono (EPFL, Lausanne, Switzerland) for providing the Albumin-Cre mice. We thank Dr Joel Haas, Pr Bart Staels and Dr Thierry Pineau for constructive discussions. We thank Dr Thierry Pineau for providing us with *Pparα*-null mice. M.R. is supported by a PhD grant from Université Paul Sabatier (Toulouse). W.W. is supported by the Lee Kong Chian School of Medicine, Nanyang Technological University Singapore start-up Grant. This work was funded by ANR "Fumolip" and "Hepadialogue" (to C.P,. D.L., N.L. and H.G.). S.E.-S., N.L., A.M. and H.G. are supported by the JPI HDHL - FATMAL. A.M., W.W., D.L., N.L. and H.G. were supported by Région Occitanie.

Author contributions

S.S., C.L., A.F., Y.L., E.F., F.L., C.N., C.B., V.B., E.M., J.B.M., A.B., T.A.S., C.C., M.T.F., S.E.S. contributed to experiments, to data analysis and to provide critical technical support. D.L., C.P., W.W., N.L. contributed to design the project, to supervise experiments and to write the paper. M.R., A.P., H.G., A.M. designed experiments, performed experiments, analysed the data and wrote the paper.

Competing interests
The authors declare no competing interests.

Additional information
Supplementary information is available for this paper at https://doi.org/10.1038/s41598-020-63579-3.

Correspondence and requests for materials should be addressed to H.G. or A.M.

Reprints and permissions information is available at www.nature.com/reprints.

Publisher's note Springer Nature remains neutral with regard to jurisdictional claims in published maps and institutional affiliations.